ELSEVIER

Journal of Nuclear Materials 250 (1997) 13–22

journal of nuclear materials

Chemical erosion behavior of graphite due to energetic oxygen impact

A. Refke *, V. Philipps, E. Vietzke

Institut für Plasmaphysik, Forschungszentrum Jülich, Association Euratom – KFA, D-52425 Jülich, Germany

Received 8 January 1997; accepted 18 July 1997

Abstract

Pyrolytic graphite, fine grain graphite and amorphous a-C:H films were irradiated with energetic oxygen in the energy range 1–5 keV between room temperature and 1800 K. CO and CO_2 molecules released during implantation were analyzed by residual and line-of-sight mass spectroscopy and their velocity distributions were determined by time-of-flight measurements. The retained oxygen was determined by thermal desorption spectroscopy after irradiation. The impact of energetic oxygen ($E > 1$ keV) on these materials results in the formation of CO and CO_2 with an erosion yield close to unity. The observed CO release behavior can be described by a local saturation model. Special experiments indicate that the underlying release mechanism is driven by ion-induced collision processes at the end of the ion trajectory of the impinging oxygen. Time-of-flight measurements have shown that released CO molecules have two different energy distributions with a thermal component corresponding to the target temperature and an overthermal component at a maximum energy of about 0.12 eV, whereas the CO_2 molecules are exclusively released with thermal energies. © 1997 Elsevier Science B.V.

1. Introduction

Due to their good thermomechanical properties and their low atomic number graphite materials are nowadays widely used for plasma facing components in fusion devices. In this way the metal impurities in the plasma are suppressed [1] and carbon and oxygen remain as main impurities.

It is well known that the bombardment of graphite with energetic hydrogen and oxygen ions leads to a chemical erosion in the form of volatile hydrocarbons [2] as well as CO and CO_2, respectively [3]. The interaction of hydrogen with graphitic materials has rather comprehensively been investigated from different points of view. Some progress has been made in modeling the hydrocarbon formation under hydrogen impact. In contrast, few experiments have been performed to investigate the chemical erosion of graphite by energetic oxygen impact. More data exist for oxidation of graphite by thermal oxygen exposure and atomic oxygen impact. As main reaction product CO is observed with a slightly temperature dependent yield and with a maximum reaction rate of 10^{-2} CO/O_2 at about 1600 K. The CO_2 production is found to be at least one order of magnitude lower than that of CO. A compilation of the results due to molecular and atomic oxygen exposure of graphite is given in [4–6].

Since the erosion yield of carbon during energetic oxygen ion impact is very high (close to unity) and nearly independent of temperature and incident ion energy [6,7], oxygen is one of the more crucial impurities in 'all carbon' fusion devices. Quantification and understanding of this erosion channel is therefore essential for the use of graphite as a material for plasma facing components.

2. Experimental set up and data evaluation

The experiments were performed in two different ion beam set-ups. In one of these the reaction products were analyzed by mass spectroscopy of the residual gas (RGA) only [7,8], whereas in another set-up the reaction products

* Corresponding author. Present address: Centre de Recherches en Physique des Plasmas, Association Euratom – Confederation Suisse, Ecole Polytechnique Federale de Lausanne, PBB–Ecublens, CH-1015 Lausanne, Switzerland. Tel.: +41-21 693 3479; fax: +41-21 693 5176; e-mail: refke@eltcv.epfl.ch.

PII S0022-3115(97)00239-0

were detected directly by a line-of-sight technique, with which also time-of-flight (TOF) measurements were done [9]. In both cases an ion beam of the ^{18}O oxygen isotope was used. This provides a much better signal-to-noise ratio of the reaction products and distinguishes the oxides formed at the target from those formed by reaction of released carbon atoms at the chamber walls.

In the RGA apparatus, which is shown in Fig. 1, the oxygen beam is produced in a plasma ion source with a cold cathode operation mode. The extracted O_2^+ beam with an intensity of 3–5 mA is mass separated in a magnetic sector field and then guided through apertures equipped with two tubes with a diameter of 2 mm, used as a differential pumping stage. In this way a pressure ratio of $\approx 10^7$ is achieved between the neutral pressure in the ion source and the detection chamber. An electrostatic lens is used to focus the beam to a diameter of < 0.5 mm at the target position. The focused beam is then scanned over an area of typically 2 mm^2 using an x–y raster scanner between the focusing lens and the target holder. To avoid the influence of secondary electrons the sample is biased with +30 V. The ion flux density is between 1×10^{14} and 3×10^{14} O^+/cm^2s (at 2 mm^2) depending on the beam energy (1–5 keV O^+). Eight samples can be mounted on a rotatable target holder allowing the change of the irradiated specimen in situ under constant ion beam conditions. In the case of RGA the signals are proportional to the particle flux from the target. To evaluate the released particle fluxes the mass spectrometer is calibrated with a known source of the relevant particle species using a calibrated gas inlet system.

Using the line-of-sight mass spectrometer technique the reaction products are detected directly without hitting the chamber wall at 45° with respect to the incident ion beam. In this technique the measured signals are proportional to the particle densities in the ionizer caused by the directly emitted flux from the target. To obtain the fluxes of released particles the signals have to be corrected with respect to the mean particle velocity. It is assumed that the particles are released with a cosine angular distribution.

Time-of-flight measurements were performed by chopping the emitted particle fluxes using a magnetically driven disk with a transmission pulse of 20 μs. The particles are then directly detected in the mass spectrometer after a flight path of 14.5 cm and collected in a multichannel counting device with a channel width of 2 μs. Further details of the line-of-sight measuring technique, the calibration and the quantitative data analysis are given in [7,12].

After implantation the retained oxygen was thermally desorbed by heating the samples ohmically up to 2000 K with a linear temperature ramp of 5–10 K/s. The target temperature was measured with infrared pyrometers. Target materials used were pyrolytic graphite (HPG99), fine grain graphite (EK98), and EK98 covered with a-^{13}C:H films of 5–60 nm thickness. The latter resembles closely the wall condition in TEXTOR after carbonization.

3. Results and discussion

3.1. Release and thermal desorption

At the beginning of the implantation with energetic oxygen ions the incident oxygen ions are completely retained in the graphite sample. With increasing oxygen fluence the incoming oxygen starts to be released from the sample in the form of CO and CO_2. The release rates of CO and CO_2 increase with the incoming oxygen fluence up to a certain saturation value. The onset of the release

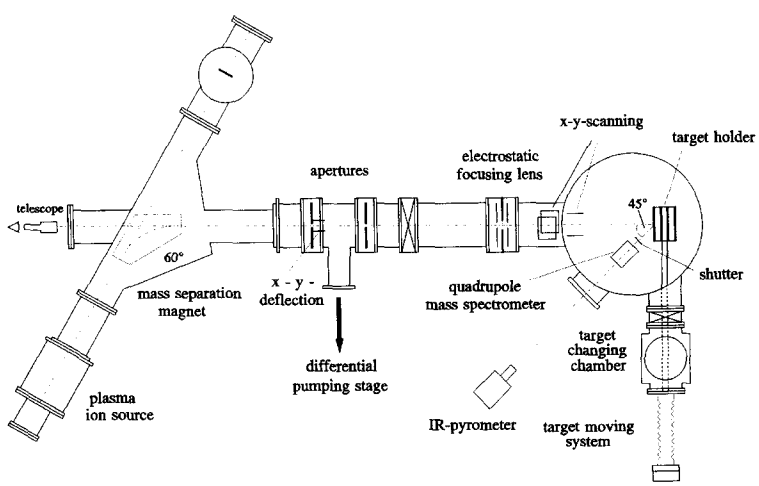

Fig. 1. Experimental set-up of the residual gas ion beam apparatus.

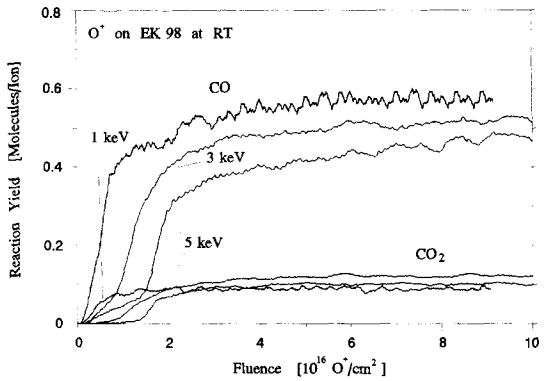

Fig. 2. Release of CO and CO_2 from EK98 irradiated with 1, 3 and 5 keV O^+ at room temperature. Incident ion flux densities were 5×10^{13}, 2.2×10^{14} and 2.6×10^{14} O^+/cm^2s respectively.

depends on the ion energy and the target temperature. This is demonstrated in Fig. 2 where the reaction yield of the released particles is shown as a function of the irradiation fluence during bombardment of EK98 at room temperature (RT) with O^+ ions of different energies (1, 3 and 5 keV). For 1 keV irradiation the release starts already after an implanted fluence of about 2×10^{15} O^+/cm^2 and then rises rapidly until the retention saturates and the release reaches a quasi steady state value. With increasing implantation energy the steep rise of the CO and CO_2 release is shifted towards higher fluences of about 8×10^{15} and 1.5×10^{16} O^+/cm^2 for 3 keV and 5 keV O^+, respectively. After an implanted fluence of $\geq 5\times10^{16}$ O^+/cm^2 the release of CO and CO_2 nearly reaches a quasi steady state in all cases. The continued slight increase of the release during further bombardment is due to formation of CO and CO_2 in a small edge zone of the irradiated area where the material saturates more slowly due to the profile of the ion beam. The steady state reaction yield reaches a value of around 0.55–0.6 for CO and 0.08–0.12 for CO_2 resulting in a total chemical erosion yield of 0.7 ± 0.05 $(CO+CO_2)/O^+$.

The retained oxygen in the graphite sample during ion implantation is released thermally in the form of CO and CO_2 by heating the target ohmically up to temperatures of about 2000 K. No desorption of atomic or molecular oxygen is observed. Fig. 3 shows the thermal desorption spectra after implantation of 3 keV O^+ in EK98 at RT for different O^+ fluences. At a given oxygen impact energy the desorption maxima of CO and CO_2 shift to lower temperatures with increasing oxygen fluence until saturation is reached. The desorption spectra are broadened towards lower temperatures but the tail at the high temperature side remains unchanged. These results can be understood if one assumes that trapping of oxygen occurs at different sites with different associated activation energies. With increasing fluence, these sites are occupied successively by the impinging oxygen, starting with those sites having the higher binding energies [8,10]. Hence, these

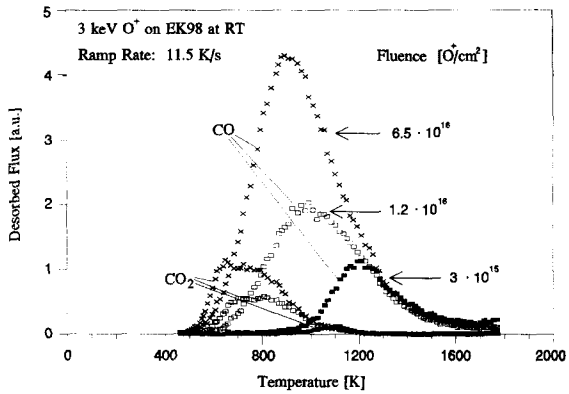

Fig. 3. Thermal desorption spectra of CO and CO_2 after irradiation with different fluences of 3 keV O^+ at room temperature. Ramp rate during thermal desorption was approximately 11.5 K/s.

desorption spectra have to be interpreted as a superposition of several desorption processes with different activation energies. This results in a much broader desorption peak than would be expected for a single binding state. When the graphite is saturated with oxygen the maxima of CO and CO_2 desorption occur at about 900 and 700 K, respectively, corresponding to mean activation energies of 2.6 eV (CO) and 2.0 eV (CO_2) if a first order desorption process is assumed [8].

Within the accuracy range of approximately ±20 K, no dependence of the desorption temperature on the implantation energy (1–5 keV O^+) has been observed. However, for small implantation fluences (corresponding to $O/C\approx$

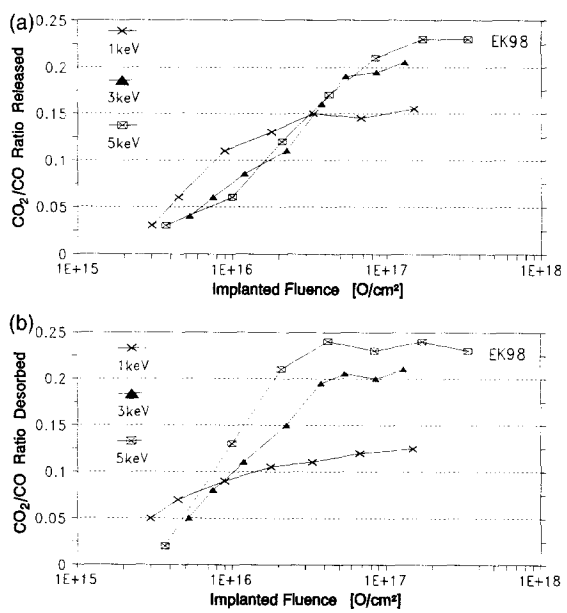

Fig. 4. Ratio of released CO_2 /CO molecules during release (a) and thermal desorption (b) as a function of O^+ ion energy and fluence.

0.1) the whole CO desorption peak is shifted towards higher temperatures with increasing energy: $T_{max} \approx 1200$ K for 5 keV and $T_{max} \approx 1050$ K for 1 keV O^+, respectively [8].

The ratio of released CO and CO_2 during irradiation and during thermal desorption depends mainly on the target temperature during irradiation [3], but also on the incident oxygen fluence and the ion energy. Fig. 4 shows this ratio of released molecules during irradiation (4a) and desorption (4b) as a function of the oxygen fluence and ion energy during irradiation at RT. In both cases a similar dependence of the CO_2/CO ratio is observed. At small fluences below 1×10^{16} O^+/cm^2 more than 90% of the released oxygen appears in the form of CO, whereas the fraction of released CO_2 increases with increasing fluence and increasing energy. Ratios of approximately 0.13 and 0.25 CO_2/CO have been measured at 1 keV and 5 keV, respectively, at fluences $> 10^{17}$ O^+/cm^2 [8].

3.2. Retention behavior

The retention behavior of oxygen in graphite is summarized in Fig. 5. The total amount of desorbed oxygen ($CO + 2 \cdot CO_2$) is shown as a function of incident fluence at different implantation energies. The retention behavior saturates above a certain fluence which increases with increasing energy. The further slight increase of the retention at fluences above the saturation value is due to the nonuniform beam profile as mentioned above. No indication of oxygen transport beyond the implantation range has been found. Assuming a uniform distribution of the implanted oxygen up to the implantation depth, a saturation value of about 0.25 O/C is obtained independent of the ion energy. This value is in good agreement with calculations of Wampler et al. [11].

3.3. Energy distribution of the reaction products

The energy distributions of the released CO and CO_2 molecules were measured by means of time-of-flight (TOF)

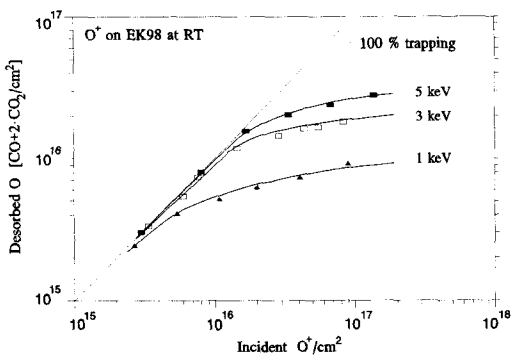

Fig. 5. Fluence dependence of the oxygen retention at room temperature shown as the amount of thermally desorbed $CO + CO_2$ for the case of 1, 3 and 5 keV O^+ irradiation.

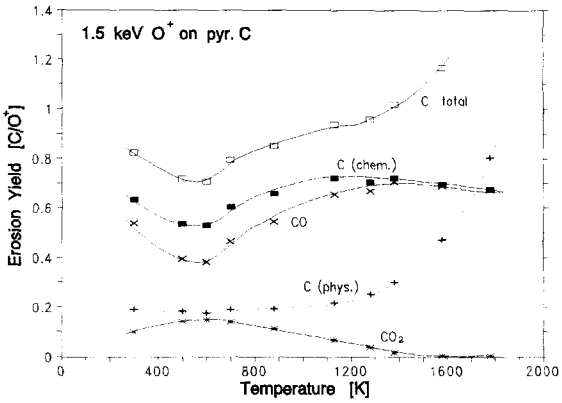

Fig. 6. Temperature dependence of the different erosion yields from pyrolytic graphite caused by 1.5 keV O^+ bombardment. The chemical erosion yields are recalculated with the energy distributions reported above. The C(phys) curve contains two contributions: physical sputtering and above 1000 K additionally RES.

during 1.5 keV O^+ ion bombardment [12]. CO is released in two different distributions: a thermal energy distribution corresponding to the target temperature and a temperature independent molecule sputtering distribution which can be fitted by a Thompson distribution [13] with an effective surface binding energy of 0.25 eV. At RT, the ratio of sputtered CO to thermally released CO amounts to 0.66. The overthermal distribution does not shift with increasing target temperature, whereas the thermal peak shifts with $T^{-1/2}$ as expected from the Maxwell–Boltzmann distribution. In contrast, the release of CO_2 can be described by a thermal distribution alone for all target temperatures investigated. A more detailed description of these observations can be found in [7,12].

3.4. Temperature dependence of the different contributions of carbon erosion by oxygen

In most previous publications on carbon erosion by energetic oxygen impact no separation of the overall erosion with respect to the different erosion processes and reaction products could be made [11,14] since the total carbon erosion yield was determined by weight loss or residual gas analysis. Fig. 6 shows a summary of the different erosion yields obtained by 'line-of-sight' detection and additional measurement of the energy of the released CO, CO_2 and C particles using the TOF technique. CO_2 is observed to have a small reaction maximum of 0.15 CO_2/O^+ at 600 K and vanishes completely at temperatures above 1400 K, whereas CO shows a corresponding minimum at 600 K and is the only chemical reaction product above 1400 K. The total chemical erosion yield shows a slight temperature dependence with a small minimum at 500–600 K and a maximum around 1100–1400 K, but remains in the whole temperature range

between 0.6 and 0.7 C/O^+. Physical sputtering of carbon atoms is independent of target temperature with a constant yield of 0.2 C/O^+ in this case (1.5 keV O^+) in good agreement with other data [15]. Above 1200 K radiation enhanced sublimation (RES) of carbon atoms sets in [16] and the total carbon release rises and exceeds unity above 1400 K. However, up to about 1600 K chemical CO and CO_2 formation remains the dominant effect under energetic oxygen ion bombardment.

3.5. Reaction mechanisms

Up to now only little knowledge exits on the details of the mechanism of CO and CO_2 formation by implantation of energetic oxygen into graphite. To improve this situation, model calculations and some special experiments were performed including postirradiation of oxygen saturated graphite with Ne^+ ions, isotope exchange experiments with $^{16}O/^{18}O$ and irradiation of ^{13}C overlaid graphite samples.

3.5.1. Neon bombardment of oxygen saturated graphite

Fig. 7 shows the CO and CO_2 release of a graphite sample (EK98) during oxygen implantation up to saturation. By switching off the oxygen ion beam after the release of CO and CO_2 has reached the saturation value, the CO and CO_2 release fluxes drop instantaneously to zero. When the oxygen bombardment is restarted after several minutes, the CO and CO_2 release fluxes resume at their original values. This indicates that the accumulated oxygen concentration remains unchanged after switching off the ion beam and causes a corresponding release when the O^+ irradiation is continued. A subsequent bombardment of the oxygen-preirradiated sample with chemically inert Ne^+ ions at the same energy (3 keV), resulting in nearly the same implantation depth of about 9 nm, leads to an instantaneous release of CO and CO_2. This release

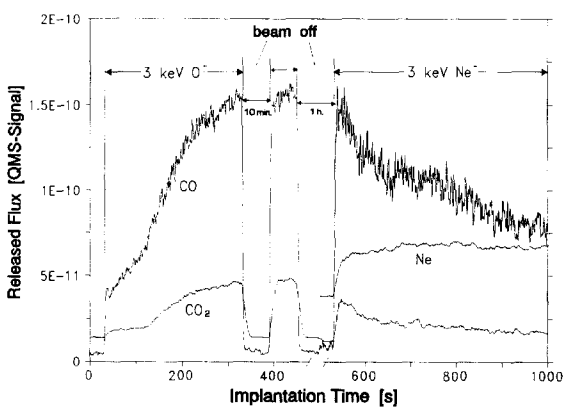

Fig. 7. Release of CO and CO_2 from graphite during 3 keV O^+ bombardment and subsequent irradiation of the O-saturated sample with 3 keV Ne^+ at room temperature.

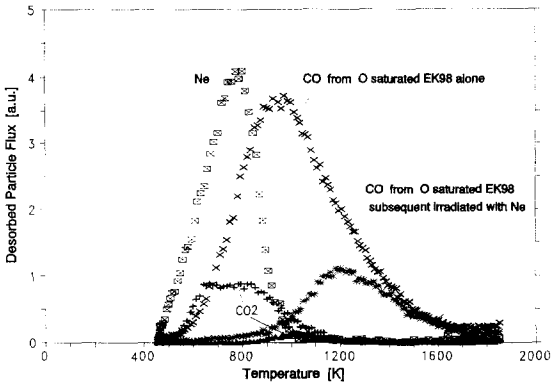

Fig. 8. Thermal desorption spectra of CO and CO_2 from O-saturated graphite alone as well as the influence of a subsequent Ne^+ bombardment. Also shown is the desorption spectrum of the implanted Ne, with a maximum at approximately 780 K.

starts at the same flux intensity as observed with O^+ bombardment and decreases then exponentially by further neon implantation. Since neon is chemically inert the release of CO and CO_2 must be due to a collision-induced process, probably detachment of a C–O complex from the graphite matrix in the collision cascade.

Some oxygen remains retained in the graphite sample even after long neon bombardment. In a subsequent heating of the sample this oxygen is released almost purely in the form of CO (see Fig. 8). The desorption peak is shifted to higher temperatures of about 1200 K similar to the temperatures observed after implantation of a small oxygen concentration. The temperature spectrum of the neon desorption, also depicted in Fig. 8, is much narrower than that of CO and the peak temperature at about 780 K is independent of the implantation fluence. This behavior resembles first order desorption [17]. Furthermore, the results indicate that graphite has a considerable retention behavior for neon.

3.5.2. Oxygen isotope exchange

Fig. 9 shows the release behavior of the different species during irradiation with the isotope $^{16}O^+$ at an energy of 3 keV onto a graphite sample at RT up to a fluence of $1.5 \times 10^{16}O/cm^2$, followed by an implantation of the isotope $^{18}O^+$ onto the same surface. After switching to the $^{18}O^+$ ion beam the released $C^{16}O$ and $C^{16}O_2$ fluxes continue to increase for a while and then decrease nearly exponentially by further $^{18}O^+$ implantation similar to the case of postirradiation with Ne^+. The onset of the $C^{18}O$ release occurs earlier compared to the $C^{16}O$ release from the previously implanted ^{16}O which is due to the already increased total oxygen concentration. Besides the formation of isotopic pure CO_2 some mixed molecules $C^{16}O^{18}O$ are formed and released, but their amount is much smaller than that of pure CO_2. At the beginning of $^{18}O^+$ bombard-

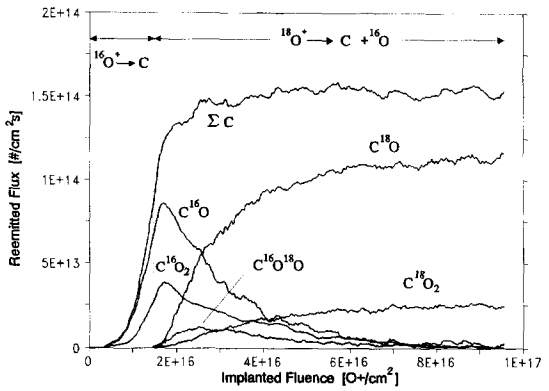

Fig. 9. Release of CO and CO_2 during successive irradiation of graphite with different oxygen isotopes at room temperature: first 3 keV $^{16}O^+$, followed by 3 keV $^{18}O^+$.

ment the release rate of the mixed CO_2 is slightly higher than that of pure $C^{18}O_2$. This can be explained assuming that the formation of the precursor for CO_2 is proportional to both isotope concentrations. No evidence exits that mixed molecules are formed by an exchange of an oxygen isotope with already formed CO_2 molecules. The sum of the chemically formed molecules shows the same release behavior as known from one oxygen isotope alone.

Both isotopes desorb thermally with similar temperature distributions, as shown in Fig. 10. If the same small amount of ^{16}O is implanted in such a sample without subsequent ^{18}O implantation, this oxygen desorbs at noticeably higher temperatures (see Fig. 3). This indicates that for a given ion energy and substrate temperature the desorption behavior is only dependent on the total retained oxygen concentration in the graphite sample. Most of the desorbed CO_2 molecules contain ^{18}O isotopes only. A small fraction consists of mixed $C^{16}O^{18}O$ molecules, while still less $C^{16}O_2$ molecules are detected. This is because

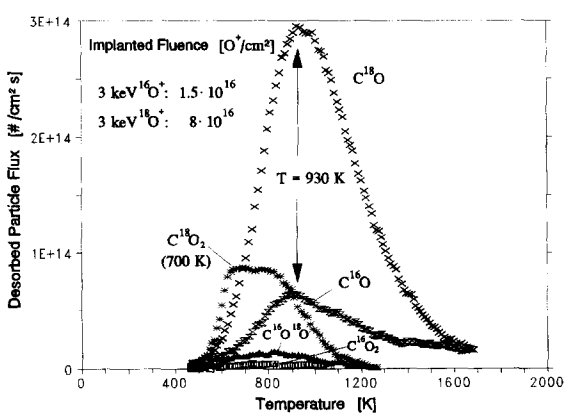

Fig. 10. Thermal desorption of the retained oxygen after successive irradiation of graphite with 3 keV $^{16}O^+$ and $^{18}O^+$ ions at room temperature.

^{16}O is less retained and the formation of CO_2 depends on both isotope concentrations as in the case of ion irradiation. Separate desorption spectra have been measured for a sample into which small fluences of the two oxygen isotopes have been implanted at different penetration depths, being 3.8 nm for 1 keV $^{16}O^+$ and 13.2 nm for 5 keV $^{18}O^+$. The measurements do not indicate any isotope mixing during the transport of the molecules from implantation depth to the surface. The amount of mixed CO_2 molecule desorption corresponds again well with the amount of both isotopes trapped within the overlap region of the implantation distributions. Therefore, it can be concluded that the formation of mixed CO_2 molecules occurs at the depth where the oxygen ions are trapped.

3.5.3. CO and CO_2 release from ^{13}C overlaid graphite

To confirm these results release and desorption measurements on ^{13}C overlaid graphite were performed. A ^{13}C layer with a thickness of 4–6 nm was deposited onto the graphite samples (EK98) in form of an a-C:H film by plasma assisted film deposition [1]. The samples were irradiated with oxygen ions of 1 and 5 keV O^+, respectively. TRIM code calculations show that the corresponding implantation profiles (assuming a Gaussian distribution) are centered at 3.8 and 13.2 nm with half widths of ± 1.5 and ± 4.7 nm, respectively. Thus, the 1 keV implanted oxygen will be trapped up to 70% within the ^{13}C layer, whereas the 5 keV O^+ ions will be distributed for more than 90% behind the ^{13}C layer as shown in Fig. 11.

Fig. 12 shows the release yields of the $^{12}CO_x$ and $^{13}CO_x$ molecules during irradiation at RT with 1 keV O^+ (12a) and 5 keV O^+ (12b). During 1 keV irradiation most of the CO_x molecules are released as ^{13}C isotopes at the beginning of the bombardment. When the release reaches 50% of the saturation value the $^{13}C/^{12}C$ ratio is about 3.2. This value agrees quite well with the calculated fractions

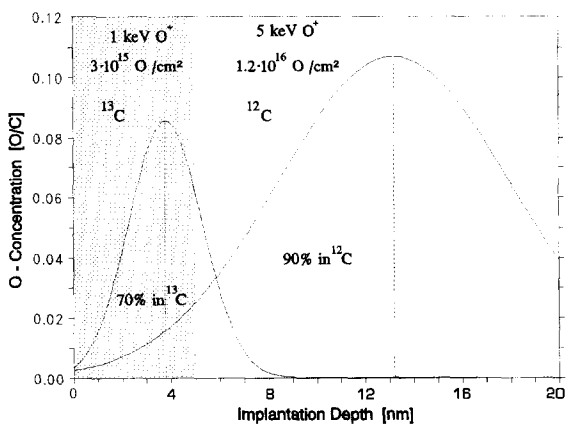

Fig. 11. Implantation profile of oxygen ions in an EK98 sample overlaid by an a-^{13}C:H film at 1 and 5 keV O^+, respectively, as determined from TRIM code calculations. The thickness of the a-^{13}C:H film is about 5 nm.

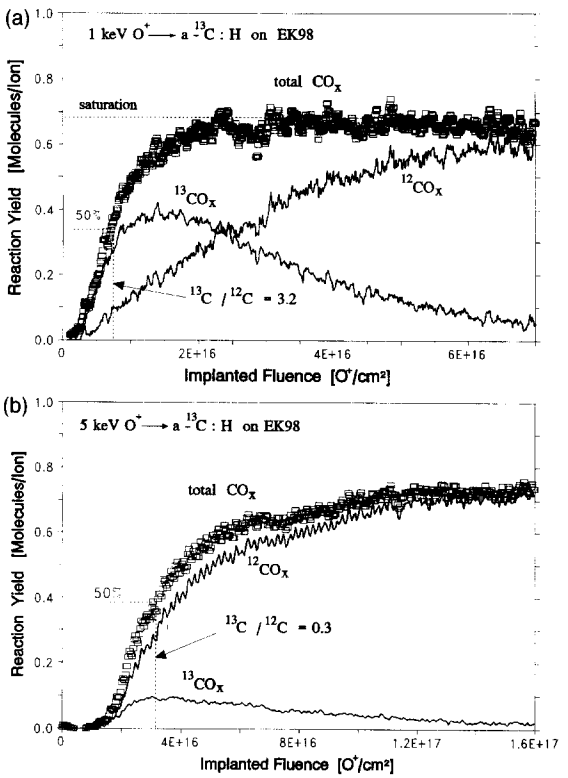

Fig. 12. Release yields of CO_x (being the sum of CO and CO_2) for the different C-isotopes during irradiation of an EK98 sample overlaid by an a-^{13}C:H film with 1 keV O^+ (a) and 5 keV O^+ (b) at room temperature. The $^{13}C/^{12}C$ ratio is given at the 50% level of the saturation value.

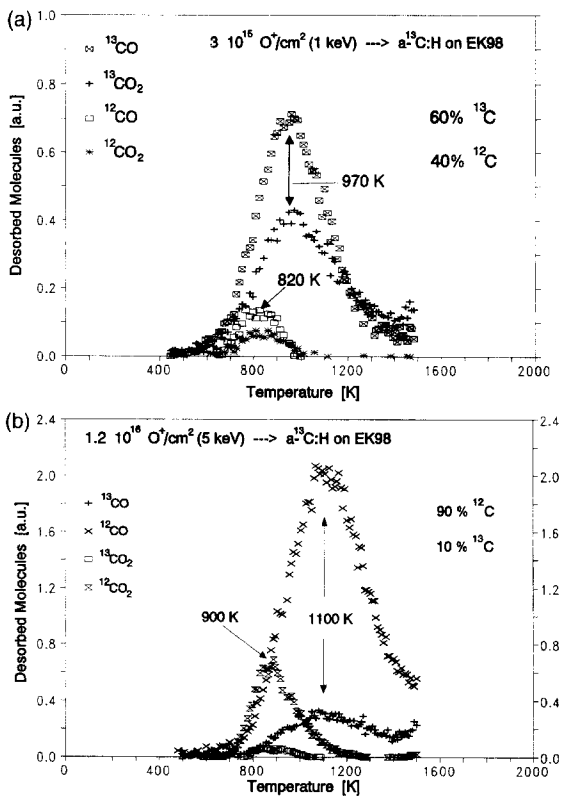

Fig. 13. Thermal desorption spectra of CO and CO_2 after 1 keV (a) and 5 keV (b) O^+ implantation in an EK98 sample overlaid by an a-^{13}C:H film.

of trapped oxygen in the different carbon layers. With increasing irradiation fluences the release yield of $^{13}CO_x$ increases further up to a maximum value of about 0.4 C/O before it decreases slowly due to the erosion of the ^{13}C layer which corresponds to an increase of the $^{12}CO_x$ release. Integrating the chemical erosion and taking into account the physical sputter yield of 0.2 C/O, a layer of 5 nm is eroded after an irradiation of about 6×10^{16} O^+/cm^2. This corresponds within the accuracy quite well with the observed release of the $^{13}C/^{12}C$ isotope ratio shown in Fig. 12a.

In contrast, most of the implanted oxygen is released in the form of $^{12}CO_x$ when the target is bombarded with 5 keV O^+ as can be seen from Fig. 12b. In this case the $^{13}C/^{12}C$ release ratio at the 50% level just reaches 0.3.

Fig. 13a and b show the distributions of the released carbon isotopes during thermal desorption after 1 and 5 keV implantation, respectively. It reflects closely the implantation distribution for both isotopes within the different layers (see Fig. 11).

3.5.4. Modeling of the oxygen retention and CO release

In case of energetic hydrogen irradiation of graphite the so called 'local mixing model' (LMM) has been developed by Doyle et al. [18]. This model has later been extended by Brice et al. [19] to describe also oxygen impact on graphite. The basic principles of the LMM are outlined in Fig. 14. It is assumed that initially all of the incoming oxygen is trapped at the end of the ion trajectory. At a certain point the local oxygen concentration reaches a saturation value S and further oxygen implantation leads to the release of oxygen. The nature of the released species is not specified in detail. If $N_O(x, t)$ denotes the atomic density of the implanted oxygen at time t and at depth x, $\phi_O(t)$ the

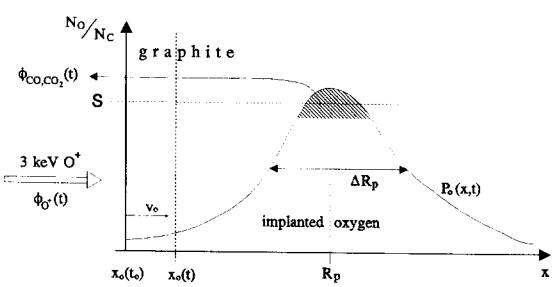

Fig. 14. Schematic view of the processes involved in the local mixing model, illustrating the oxygen retention and reemission during O^+ irradiation of graphite. Symbols are explained in the text.

incoming flux density of the O^+ ions at the surface at $x_O(t)$ and $P_O(x, t)$ the normalized oxygen implantation profile, the time evaluation of the oxygen concentration is described by the rate equation

$$\frac{dN_O}{dt} = \phi_O(t)P_O(x, t) - \nu_O N_O(x, t)\,\delta(x - x_O(t)), \tag{1}$$

where $\nu_O = dx_O/dt$ is the velocity of surface erosion and $\delta(x - x_O(t))$ is the delta function, taking into account the shift of the actual surface due to erosion. The above formula describes the local erosion behavior as long as saturation is not reached, which means that $N_O < SN_C$, with $N_C(x, t)$ the density of carbon atoms and $S = (N_O/N_C)$ the saturation value. The first term on the right hand side describes the rise of the oxygen concentration due to ion implantation, while the second term represents the loss of oxygen inventory due to surface erosion by means of physical sputtering. This results in a continuous change of the implantation profile $P_O(x, t)$ during the irradiation. A more detailed description also has to take into account the change of the target composition due to the ion implantation [19], but is not considered within this paper.

In order to describe our data the local mixing model has been slightly modified using the following assumptions: first, carbon and oxygen atoms are physically sputtered from the surface with a yield of ≈ 0.3 (in case of 3 keV O^+ [15]); second, the implanted oxygen is released in the form of CO_i ($i = 1,2$) with a chemical erosion yield K_i and a flux intensity which is proportional to the incident ion flux density ϕ_O and the existing oxygen concentration N_O. Hence, the following expression for the released CO_i flux densities is used:

$$\phi_{CO_i}(t) = K_i(t)\phi_O(t)N_O(t)/(N_C S). \tag{2}$$

When the target is saturated up to the implantation depth, we obtain $N_O/(N_C S) = 1$ and the released fluxes ϕ_{CO_i} become constant:

$$\phi_{CO_i} = K_i\phi_O, \tag{3}$$

where $K_1 \approx 0.6$ and $K_2 \approx 0.1$ are the measured values for the chemical erosion yields of CO and CO_2, respectively.

During the built-up phase of the oxygen concentration the released CO_i flux is obtained by integration over the whole implantation depth. This gives

$$\phi_{CO_i}(t) = \frac{K_i(t)\phi_O(t)}{N_C S}\int N_O(x, t)\,dx. \tag{4}$$

Furthermore, the surface erosion due to sputtering can be expressed as

$$\nu_O = \frac{dx_O}{dt} = Y_C(E)\frac{\phi_O}{N_C}, \tag{5}$$

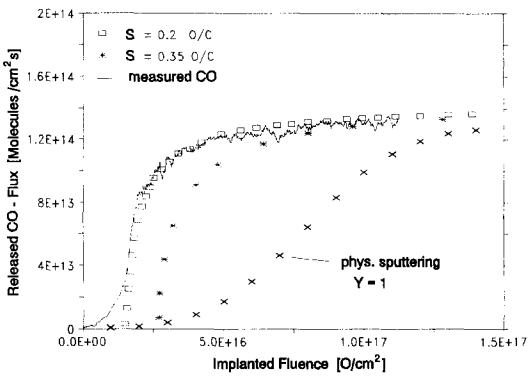

Fig. 15. Calculated CO release from the local mixing model for saturation values of $S = 0.2$ and 0.35 O/C compared with experimental results during 3 keV O^+ irradiation of graphite. Also shown are the results of a sputtering mechanism (with a yield of unity) that only takes into account the release of CO once the sputter front has reached the position of the implanted oxygen.

with $Y_C(E)$ the energy dependent sputtering yield and N_C the atomic density of the carbon matrix. Using Eqs. (4) and (5) in Eq. (1), the temporal behavior of the total flux density of the chemically released CO_i molecules is finally given by

$$\phi_{chem}(t) = \sum_i \phi_{CO_i}(t) = \frac{K_1 + K_2}{N_C S}\phi_O^2 \iint \times \left[P_O(x, t) - \frac{Y_C(E)}{N_C}N_O(x, t)\delta(x - x_O(t))\right] \times dx\,dt. \tag{6}$$

The saturation concentration S can be used as a parameter to fit the measured data to the release behavior calculated from Eq. (6). This is shown in Fig. 15 for the case of 3 keV O^+ irradiation of graphite (EK98) at RT. The figure shows the result for two saturation values S. The observed release behavior can be reasonably fitted using a saturation value of about 0.2 O/C. In addition, the release of CO can be calculated under the assumption that all of the incident oxygen is trapped at the implantation depth and that the oxygen is released in the form of CO as soon as the layer in front of the implanted oxygen is physically sputtered away, i.e., the sputter front has reached the position of the implanted oxygen. As can be seen in Fig. 15, this process alone cannot explain the transient release behavior of CO, even when a rather high sputter yield of $Y_C = 1$ is assumed.

3.5.5. Release mechanism, transport and energy distribution of the reaction products

As already mentioned, up to now no comprehensive model exits which can explain the mechanism of CO and

CO_2 formation and release due to O^+ bombardment of carbon. However, our results suggest the following picture: the implanted oxygen ions are trapped at the end of the ion trajectory at free active carbon sites at which C–O complexes are formed as precursors. The sticking probability is nearly unity and therefore no drastic temperature and energy dependence is observed. At least two kinds of C–O complexes appear to exist which are formed already during the ion implantation. These conclusions can be drawn from the shape of the desorption spectra and the distribution of the CO/CO_2 molecules obtained during a second heating ramp when a first desorption is stopped at a temperature at which almost all CO_2 is already released whereas the CO desorption is not yet started. During the second heating ramp no further desorption of CO_2 occurs. The desorption of CO starts at the final temperature of the first ramp and shows for higher temperatures an identical desorption behavior as during an uninterrupted desorption procedure. With increasing oxygen fluence the trapping sites are filled up, the oxygen concentration rises and CO and CO_2 molecules are more and more released by collision processes with incoming beam ions. This two-step formation of the oxygen containing complexes at the end of the ion trajectory and the subsequent ion induced release of CO and CO_2 are demonstrated by the CO and CO_2 formation during postirradiation with chemically inert Ne ions, as well as by changeover between irradiation with different oxygen isotopes and by irradiation of ^{13}C overlaid graphite.

The formed CO and CO_2 molecules are volatile and are transported through natural pores or microchannels, which are already created due to the ion irradiation, to the outer surface from which they leave the substrate. The experiments presented in this paper indicate that the release rate of the volatile reaction products is not determined by a diffusive process [7].

When the saturation level is reached the oxygen is homogeneously distributed up to the implantation depth. The saturated oxygen concentration is found to be 0.25 O/C, similar to that of oxygen chemisorption on the edges of pyrolytic graphite with a high chemisorption rate, which is measured to be 0.33 O/C [6]. No indications for an inward diffusion of the implanted oxygen are obtained, probably due to the low diffusion rate of oxygen. The transport of oxygen within the irradiated graphite may occur almost in the form of CO molecules which penetrate to the outer surface mainly through the microchannels. Furthermore, since the irradiated samples are getting more and more amorphous as a result of the ion bombardment, the reaction yields of oxygen erosion become equal for the various types of graphite investigated (pyrolytic graphite (HOPG99), fine grain graphite (EK98) and a-C:H films).

Fig. 16 illustrates our present view in a schematic way: several different C–O complexes (precursors) are formed during oxygen bombardment and the CO and CO_2 molecules are released by the kinetic impact of incoming oxygen ions. The initially released molecules may thus

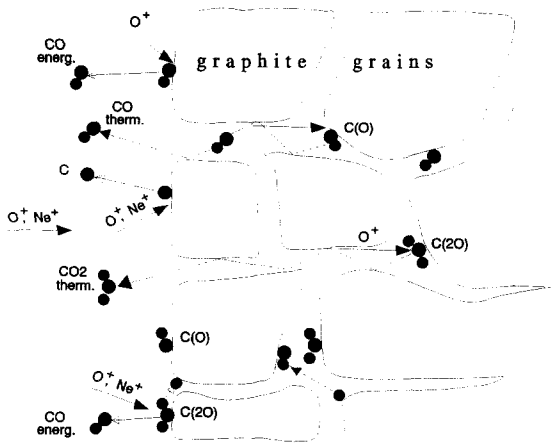

Fig. 16. Schematic view of the release mechanisms of CO and CO_2 during irradiation of graphite with energetic oxygen ions: the carbon oxide molecules are formed from different C–O precursors on active sites at inner surfaces within the implantation region of the irradiated sample. They are subsequently released by further ion impact due to an ion-induced process and then transported through microchannels to the surface from where they are desorbed. Most of them are thermalized during their transport to the surface. Those molecules which are released directly at or near to the surface can show an overthermal energy distribution due to a molecule sputtering process.

have an overthermal kinetic energy distribution but the majority is thermalized during transport to the material surface. These molecules are released with a thermal energy distribution corresponding to the target temperature. Other molecules located close to the surface may be directly released by a collision mechanism and are emitted with an overthermal energy distribution which can be described by a Thompson distribution assuming some fictive surface binding energy. However, the binding energy is very low and the energy of the emitted overthermal CO molecules (≈ 0.12 eV) lies between that of physically sputtered atoms ($\simeq 1$ eV) and thermally released molecules ($\simeq 10^{-2}$ eV). Thus we might speculate that a somewhat more complex reaction mechanism is responsible for the overthermal molecule release. Ion induced processes, i.e., bond breaking or reaction with ion induced point defects, can cause a rearrangement of some C–O complexes and hence a transfer of kinetic energy to the formed CO molecules. Moreover, part of the kinetic energy received during the collision process can be converted into internal energies of the molecule (rotational or vibrational excitation) [20]. In contrast to CO, no overthermal CO_2 molecules are observed which might be explained by a breakup of CO_2 during the sputter process at the surface. Thus, more analysis is necessary to interpret the observed energy distribution of emitted CO and CO_2 molecules.

4. Summary

Chemical erosion of graphite by impact of energetic oxygen was analyzed by means of mass spectrometry using $^{18}O^+$ ion beam irradiation in the energy range of 1–5 keV O^+. It was found that the implanted oxygen is retained in the graphite until a certain fluence is reached above which the oxygen is released in the form of CO and CO_2 with a gradually increasing yield. In steady state the sum of the CO and CO_2 release yields is about 0.7 with no pronounced temperature and energy dependence in the range from RT to 1800 K and 1 to 5 keV O^+, respectively. No reemission of atomic or molecular oxygen was detected. When the release of CO and CO_2 saturates, the oxygen concentration in the graphite reaches at RT a saturation value of about 0.25 O/C. This value is constant in the investigated energy range but decreases with increasing target temperature.

During a thermal desorption procedure, the retained oxygen is completely released in the form of CO and CO_2 with desorption maxima at ≈ 900 and ≈ 700 K, respectively. The ratio of released CO_2/CO covers the range between zero and a maximum value of 0.25 and increases with increasing implantation fluence and ion energy. This ratio is similar for both the irradiation induced release and thermal desorption.

Special experiments were performed to analyze the formation mechanism of CO and CO_2 by postirradiation of oxygen saturated graphite with Ne^+ ions, isotope exchange irradiation with $^{16}O/^{18}O$ ion beams and irradiation of ^{13}C overlaid graphite with oxygen ions at different energies. The results show that the dominant release mechanism of CO and CO_2 is an ion-induced collision process. The released flux density is proportional to the local oxygen concentration and the incoming ion flux density. The molecule formation occurs at the end of the ion trajectory where the implanted oxygen is trapped at several active sites and forms different C–O complexes as precursors of CO and CO_2. From these sites the oxygen is released as CO and CO_2 molecules by subsequent ion-induced collision processes. The molecules are transported from the end of ion range to the target surface. Thermal diffusion does not appear to determine the transport of the molecules to the surface and an ion-induced transport mechanism is likely. The observed release behavior can be described by an extended local saturation model.

Time-of-flight measurements have shown that the released CO molecules have both a thermal and an overthermal energy distribution, whereas the CO_2 molecules are only released with thermal energies. The energy distribution of the fast CO component has a maximum at about 0.12 eV independent of the target temperature, but the relative flux of these overthermal CO molecules decreases with increasing temperature. The release of such overthermal molecules from plasma facing components leads to a higher penetration of those particles into the edge plasma of fusion devices and therefore influences their ionization and transport processes within the plasma. Although the complex mechanism of the molecule sputtering process is not yet completely understood, a simple model of CO formation and release has been developed from our results.

References

[1] J. Winter, J. Nucl. Mater. 145–147 (1987) 131.
[2] E. Vietzke, V. Philipps, Fusion Technol. 15 (1989) 108.
[3] E. Vietzke, T. Tanabe, V. Philipps, M. Erdweg, K. Flaskamp, J. Nucl. Mater. 145–147 (1987) 425.
[4] P.L. Walker Jr., R.L. Taylor, J.M. Ranish, Carbon 29 (3) (1991) 411.
[5] N.R. Laine, Carbon 29 (6) (1991) 729.
[6] E. Vietzke, A.A. Haasz, in: Physical Processes of the Interaction of Fusion Plasmas with Solids (Academic Press, New York, 1996) p. 135.
[7] A. Refke, PhD Thesis, KFA Jülich, Report Jül-2995 (1994).
[8] A. Refke, V. Philipps, E. Vietzke, J. Nucl. Mater. 212–215 (1994) 1255.
[9] E. Vietzke, K. Flaskamp, M. Hennes, V. Philipps, Nucl. Instrum. Meth. B2 (1984) 617.
[10] G. Tremblay, F.J. Vastola, P.L. Walker, Carbon 16 (1978) 35.
[11] W.R. Wampler, D.K. Brice, J. Vac. Sci. Techn. A4 (1986) 1186.
[12] E. Vietzke, A. Refke, V. Philipps, J. Nucl. Mater. 220–222 (1995) 249.
[13] M.W. Thompson, Philos. Mag. 18 (1968) 377.
[14] E. Hechtl, J. Bohdansky, J. Nucl. Mater. 141–143 (1986) 138.
[15] W. Eckstein, C. Garcia-Rosales, J. Roth, W. Ottenberger, Sputtering Data, Report IPP Garching 9/82 (1993).
[16] V. Philipps, E. Vietzke, H. Trinkaus, J. Nucl. Mater. 179–181 (1991) 25.
[17] P.A. Redhead, Vacuum 12 (1962) 203.
[18] B.L. Doyle, W.R. Wampler, D.K. Brice, J. Nucl. Mater. 93&94 (1980) 551.
[19] D.K. Brice, W.R. Wampler, J. Nucl. Mater. 145–147 (1987) 368.
[20] H.M. Urbassek, Nucl. Instrum. Meth. B18 (1987) 587.